INTERNATIONAL JOURNAL OF CLIMATOLOGY
RMetS Royal Meteorological Society

Inter-decadal variability in potential glacier surface melt energy at Vestari Hagafellsjökull (Langjökull, Iceland) and the role of synoptic circulation

Journal:	*International Journal of Climatology*
Manuscript ID:	Draft
Wiley - Manuscript type:	Research Article
Date Submitted by the Author:	n/a
Complete List of Authors:	Matthews, Tom; National University of Ireland, Geography Hodgkins, Richard; Loughborough University, Geography Guðmundsson, Sverrir; University of Iceland, Institute of Earth Sciences Pálsson, Finnur; University of Iceland, Institute of Earth Sciences Björnsson, Helgi; University of Iceland, Institute of Earth Sciences
Keywords:	Glacier melt modelling, Glacier surface energy balance, Synoptic circulation, North Atlantic Oscillation, Greenland Blocking Index

Inter-decadal variability in potential glacier surface melt energy at Vestari Hagafellsjökull (Langjökull, Iceland) and the role of synoptic circulation

Matthews[1] T, Hodgkins[2] R, Guðmundsson[3] S, Pálsson[3] F, Björnsson[3] H

[1]Department of Geography, National University of Ireland, Maynooth

[2]Department of Geography, Loughborough University, UK

[3] Institute of Earth Science, University of Iceland, Iceland

Corresponding author:

Tom Matthews

Department of Geography

National University of Ireland

Maynooth

Kildare

Republic of Ireland

e-mail: tom.matthews@nuim.ie

Key words: Glacier melt modelling; Glacier surface energy balance; Synoptic circulation; North Atlantic Oscillation; Greenland Blocking Index

Abstract

The Surface Energy Balance (SEB) of glaciers, although of considerable importance for understanding the melt response to climate change, is generally analysed only for brief time periods due to the logistical challenges of meteorological measurement campaigns on glaciers. Insight into low-frequency changes in the SEB in response to climate warming and variable atmospheric circulation patterns has thus been limited. Here this problem is addressed by using ERA-Interim reanalysis data to extend glacier-meteorological records at two locations on Vestari Hagafellsjökull for the period 1979-2012. Trend analysis is conducted for this series before the role of synoptic circulation in modulating surface energetics is investigated. The results indicate that potential melt energy has increased significantly throughout the period of simulation at both locations, with the largest increase evident for the turbulent heat fluxes. The synoptic conditions associated with the recent high melt rates on the proximate Greenland Ice Sheet (GrIS) do not manifest as similarly extreme melt conditions for our Icelandic location. We also find that the North Atlantic Oscillation Index is significantly correlated with components of the SEB. This association remains hidden if the melt rate is assessed in isolation, highlighting the utility of the SEB approach presented here for assessing synoptic aspects of glacier-climate interactions.

1. Introduction and aims

Melting of the Earth's terrestrially-stored ice is of the utmost hydrological and societal importance. Glaciers and ice caps play a critical role in modulating the seasonal hydrology of mountainous catchments (Jansson et al., 2003; Bradley et al., 2006) and their melting has contributed substantially to recent sea-level rise (Meir et al., 2007; Jacob et al., 2012). Hence, there is a need to understand and quantify the response of the cryosphere to the effects of climate change.

Critical to the rate at which glaciers and ice caps lose mass is the SEB. That is, the net balance of energy at the glacier surface: surplus energy drives melting once the surface has been warmed to 0°C. Much research has addressed the measurement and simulation of the SEB in different climatic environments (e.g. Oerlemans, 2000; Klok and Oerlemans, 2002; Hock and Holmgren, 2005; Giesen et al., 2009; Guðmundsson et al., 2009; Six et al., 2009; Sicart et al., 2011). Such investigations are often used to identify the relative importance of different energy fluxes in driving melting (e.g. Giesen et al., 2009; Nicholson et al., 2012), to calibrate empirical glacier melt models (e.g. Braithwaite, 1995; Arendt and Sharp, 1999; Matthews et al. 2014), or to assess the sensitivity of glacier melt to prescribed increases in air temperatures (e.g. de Wildt et al. 2004; Björnsson et al., 2005). SEB studies therefore play a critical role in understanding how the prevailing weather drives surface melting, and ultimately, the response of glaciers to climate change.

To evaluate the SEB, micrometeorological data from the glacier boundary layer are required. This, however, presents a serious logistical challenge on glaciers, as the remote location and harsh climate typical of glacierized terrain makes continuous data acquisition difficult. As a consequence SEB studies are often brief in duration, which is problematic because the representativeness of such short-term investigations may be limited: the sampling interval may not represent the full range of SEB conditions experienced at the study location. For instance, interannual changes in the frequency and duration of particular weather types (Brazel et al., 1992; Hannah et al., 1999; Konya and Matsumoto, 2010), might result in observations from a short-lived observation campaign being misleading regarding 'average' conditions.

Brief SEB investigations are particularly limiting for studies which seek to explore the synoptic dimension to surface energetics. In general, relatively few researchers have considered this aspect of glacier-climate interactions from an energy-balance perspective (Hay and Fitzharris, 1988; Brazel et al., 1992; Hannah et al., 1999). Studies at interannual resolution are particularly sparse, yet such focus is much required, as an understanding of how large-scale, low-frequency atmospheric processes ultimately drive melting at the glacier-scale is important to establish the likely future response of glaciers to climate change. The micrometeorological processes which ultimately drive surface energy transfer vary at too small a scale to be resolved by spatially-coarse climate models, and coupling the small- and large-scales provides a means to address this scale mismatch. A reminder of the importance of synoptic circulation in modulating glacier-surface energetics has been provided by studies of the GrIS. Recent research in this region (Fettweis et al., 2011, 2012; Hanna et al., 2013, 2014) has emphasised the role of unprecedented high pressure over the western flank of the GrIS in driving high, and indeed, record-breaking melt rates over the ice sheet.

One way of extending SEB investigations to a length which is more appropriate for exploring synoptic controls on the surface energetics, is to calculate the SEB using meteorological data recorded at weather stations located off-glacier (e.g. Klok and Oerlemans, 2002). However, the low spatial density of such climate-monitoring stations (Jarosch et al., 2012) means that using these records in place of glacier observations is not a practical solution for studying the

SEB of many of the world's glaciers and ice caps. In this regard, though, gridded reanalyses products may provide a solution.

Reanalyses data have their origins in weather forecast initialization. Produced for a regular grid of global coverage by combining raw climate observations with the results of a short-term weather forecast to produce the best estimate of the atmospheric state, they can provide a useful means of gaining insight into meteorological variability in data-sparse regions. In a glaciological capacity, reanalysis data have been used previously to force both temperature-index mass balance models (e.g. Radić and Hock, 2006; Zhang et al., 2007) and energy balance mass balance models (e.g. Hock et al., 2007; Rye et al., 2010), but have been used rarely as a means to extend SEB investigations beyond periods of in-situ observations.

In the present study we pursue two main aims related to the points raised above: the first is to assess the feasibility of substituting reanalysis data in place of direct in-situ observation for the purpose of SEB simulation; the second is to establish the role of synoptic circulation in modulating interannual change in the simulated surface energetics. In combining these aims, we seek to demonstrate the value of the bias-corrected reanalysis data for extending SEB series.

2. Data and Methods

2.1 Overview

The general approach taken here is to use in-situ meteorological data recorded at AWSs to adjust reanalysis data to the glacier climate. Melt energy simulated by a SEB model driven with these data is then compared with the results from a SEB model forced with in-situ AWS data. Close agreement between the two series is taken as confirmation that the reanalysis data can be used to hindcast the SEB (aim 1), which is subsequently undertaken for the duration of the reanalysis series. The resulting SEB record is then analysed, with specific attention paid to the role of atmospheric circulation in modulating surface energetics (aim 2).

2.2 Study Location and meteorological observations

In-situ meteorological data were obtained from Vestari Hagafellsjökull, an outlet glacier of the Langjökull Ice Cap in Iceland (Figure 1). The climate of Iceland is influenced by the proximate GrIS (~400 km away) and by warm and cold ocean currents which meet of its shores (Hanna et al., 2004). The warm Irminger Current encircles the south, west and north of the island, whilst the cold East Iceland current (a branch of the East Greenland Current) flows south-easterly of Iceland's east coast. The polar front is also normally in close proximity, meaning that air mass transitions are frequent and atmospheric dynamics have a profound effect on Iceland's climate (Einarsson, 1984; Wang and Rogers, 2001; Hanna et al., 2004). These characteristics make our study site well-suited to examining the role of synoptic circulation on surface melt processes. Moreover, given the role of circulation anomalies in driving the unprecedented melt rates observed recently on the proximate GrIS, our record presents the opportunity to explore the extent to which a coherent melt response to synoptic forcing occurs in this region of the North Atlantic.

On Vestari Hagafellsjökull, we used data from two AWSs. These stations, located at 500 m and 1100 m (hereafter VH 500 and VH 100, respectively: see bottom right of Figure 1), are described in Guðmundsson et al. (2009) and Matthews et al. (2014). Observations from the AWSs were employed from June-August (hereafter JJA) 2001 to 2007 at VH 500 and JJA 2001-2009 at VH 1100.

2.3 Reanalysis data

To extend the SEB series, the ERA-Interim dataset was used, which is the latest reanalysis product from the European Centre for Medium Range Weather Forecasting, succeeding the ERA-40, and spanning the period 1979-present (see Dee et al. (2011)). As input to our SEB model (described below) the incident radiative fluxes (shortwave and longwave), two-metre air temperature, two-metre vapour pressure, and two-metre wind speed are required; appropriate variables were therefore extracted from the ERA-Interim archive (http://dataportal.ecmwf.int/data/d/interim daily/) at 0.75° × 0.75° resolution for the four grid points closest to our study site (see Table 1). The average height of the reanalysis terrain across these points is 375 m. The extracted variables were then bilinearly interpolated to the location of the AWSs (cf. Radić and Hock, 2006; Rye et al. 2010). All reanalysis data were extracted at three-hourly resolution for the JJA period 1979-2012, before being post-processed to daily means.

Comparison of the interpolated reanalysis variables with the in-situ observations indicates appreciable bias (Figure. 2). We therefore adjusted the reanalysed meteorological variables to the glacier using a quantile-mapping approach (Rye et al., 2010; Hashino et al., 2007). This non-parametric technique for bias correction has been found to be superior to other statistical transformations in comparative studies (Hashino et al., 2007; Gudmundsson et al., 2012). The procedure was implemented via a direct one-to-one mapping of rank-ordered pairs for the period of coincident observation at each AWS. Outside this interval, the reanalysis variables were corrected by linearly interpolating between pairs. Values beyond the range witnessed during the overlapping period are corrected by the minimum/maximum correction factors, as appropriate. Although this practice is common (Boé et al., 2007; Rye et al., 2010; Themeβl et al., 2012; Gudmundsson et al., 2012), it is questionable if temporal trends mean that these minimum/maximum corrections need to be applied often. In such instances, it is recommended to remove these trends prior to implementing quantile mapping (Beyene et al., 2010; Dobler et al., 2012). However, this is not an issue here because across all variables and both locations, a maximum of ~0.3% of the reanalysis series (vapour pressure at VH 1100) were subject to these extreme correction factors.

Whilst quantile mapping corrects for biases in the reanalysis data, it does not affect the temporal agreement with the meteorological variables measured on glacier. This was assessed in the present study by calculating correlation coefficients between the quantile-mapped reanalysis data and the observed glacier meteorology.

2.4 Surface Energy Balance

The suitability of the SEB model specification employed here (Table 2) has been demonstrated in previous research (Matthews, 2013; Matthews et al., 2014). We ran this model at hourly resolution using meteorological data recorded at the glacier AWSs to generate reference SEB series for each location. When the model was forced with the bias-corrected reanalysis data, we performed two experiments. The first was designed to validate the SEB series generated with the reanalysis data. For this, the model was run at daily resolution for the period when the AWSs were operational with the measured albedo and emitted longwave radiation used to resolve the net radiative balance. This treatment isolates the effect of different meteorological forcing data (in-situ *versus* reanalysis) on model performance. We refer to the SEB series generated with in-situ meteorological data as 'REF', and use 'REANv', to denote the series obtained using the reanalysis data from this experiment. Validation of REANv was achieved by comparing this series with water equivalent melt totals derived from the daily mean energy fluxes in the REF series. Comparisons were made at daily and annual resolution and correlation coefficients were used to quantify the agreement between series.

186 The second experiment was a hindcasting one, in which the energy balance for the entire 34-
187 year JJA period was calculated. For this, the albedo was held constant as the mean observed
188 at each AWS during the observational period, and the emitted longwave radiation was
189 assumed equal to a blackbody at the melting point. In the case of negative energy balances,
190 all fluxes were set to zero and no melt was assumed. The SEB series resulting from this
191 experiment is denoted 'REANh' hereafter. By holding the glacier-surface properties constant
192 this experiment isolates the role of changes in the prevailing weather in driving SEB
193 variability. The aim of this approach is not to produce the most accurate simulation of the
194 SEB over the period 1979-2012, but to assess the long-term variability of potential melt
195 energy, attributable only to changes in the prevailing weather. By conducting our SEB
196 experiment according to the above conditions, we could isolate this control on surface
197 energetics.

198 Trends in REANh were calculated using least-squares linear regression following Box (2002)
199 and Hanna et al. (2004), with the significance of the slope coefficients (trends) determined
200 via a two-tailed *t*-test. This treatment therefore only considers sampling uncertainty in
201 evaluating significance; it makes no provision, for uncertainty stemming from the use of
202 reanalysis data to calculate REANh, or from the structure of the SEB model itself.

203 **2.5 Atmospheric circulation**

204 The role of atmospheric circulation in driving interannual variability in potential melt energy
205 was assessed by examining the height fields of the 900 hPa surface, and by correlating melt,
206 and the individual SEB components from REANh, with the North Atlantic Oscillation Index
207 (NAOI: JJA Hurrel Principal-Component based index; data provided by the Climate Analysis
208 Section, NCAR, Boulder, USA, and downloaded from:
209 http://climatedataguide.ucar.edu/guidance/hurrell-north-atlantic-oscillation-nao-index-pc-

based) and the Greenland Blocking Index (GBI). Following Hanna et al. (2013), the GBI was defined as the mean JJA 500 hPa geopotential height over a region extending from 60-80°N and 20-80°W. For both the 900 and 500 hPa surfaces, JJA height fields were obtained at twice-daily resolution from the ERA-Interim archive.

Prior to analysing the role of synoptic circulation in modulating surface energy exchange, all series (REANh, the 900 hPa height field, and the NAOI/GBI indices) were detrended via linear regression. This was deemed necessary because average northern hemisphere air temperatures have risen appreciably during the period 1979-2012 (e.g. Jones et al., 2012), and such warming (which can enhance the temperature-dependent heat fluxes of the SEB and raise atmospheric pressure surfaces) may result in spurious associations between the SEB and atmospheric circulation patterns if not accounted for.

The 900 hPa surface was used because this provides information of atmospheric flow at a level close to the AWSs (mean atmospheric pressure during the observational period was 950 hPa and 883 hPa at VH 500 and VH 1100, respectively). The relationship between the 900 hPa flow field and REANh was determined by plotting anomaly maps for the five years with the highest melt rates. These years were identified by ranking melt *z*-scores averaged between elevations, so that equal weight was given to both locations when defining high melt years. We also correlated the 900 hPa height field with REANh to determine linear dependencies of the SEB on the synoptic flow.

The GBI and the NAOI were used to explore the relation between surface energetics and synoptic climatology because these indices have been identified as useful indicators of both GrIS melting (Hanna et al., 2013) and interannual climatological variability in Iceland (Hanna et al., 2004). All correlations between components of REANh and synoptic climate indices/flow field were performed at annual (JJA) resolution. Unless otherwise stated, all correlations cited in the text are termed 'significant' if they have a p-value less than 0.05.

3. Results

3.1 Reanalysis climatology

Correlation coefficients quantifying the linear agreement between reanalysis and AWS variables are provided in Table 3. Generally, correlations are strong for all locations, and all are highly significant. Wind speed at VH 500 registers the lowest agreement. However, empirical associations between glacier wind speeds and other near-surface meteorological variables have been noted in Icelandic studies (Björnsson et al., 2005), so we attempted to improve the correspondence between the bias-corrected reanalysis and observed wind speeds by regressing wind speed residuals on other reanalysis variables (see Table 4). The resulting regression model improved the agreement between the corrected reanalysis wind speed and that measured at VH 500 (new r = 0.61)

3.2 Surface Energy Balance Modelling

Simulating the SEB using the corrected reanalysis data to drive the melt model resulted in good agreement between the observed and simulated heat fluxes at both daily and annual resolution (Table 5 and Figure 3). The least agreement between series is observed for the latent heat flux at VH 500 when assessed at annual resolution. However, given its relatively minor role in the SEB (Table 5), this does not propagate substantially to the skill in capturing total melt at either elevation. Table 5 also indicates that the bias-correction routine ensures that the relative importance of each of the energy fluxes within the SEB is reproduced closely.

Having established the agreement between SEB simulations forced with the in-situ observations and the corrected reanalysis data, the SEB was calculated for the entire 34-year period. The glacier-surface properties (surface roughness, albedo, the outgoing longwave flux) were held constant for this experiment: changes in simulated melt energy during the hindcasting period are therefore entirely the result of variability in the prevailing weather.

Examination of the resulting SEB series and their trends (Figure 4 and Table 6) indicates that potential melt energy has increased significantly throughout the period 1979-2012. At both locations, the sensible, latent and shortwave heat fluxes have contributed positively to the increase in total melt energy, whilst the longwave heat flux has remained essentially unchanged. The relative importance of the different energy fluxes within the SEB also shows appreciable interannual variability (Figure 5), which is, in some cases, systematic. For example, the percentage of potential melt energy provided by the turbulent heat fluxes has increased over the hindcasting interval (Figure 6) at a rate which is significant. Thus, the turbulent heat fluxes have become relatively more important within the SEB during this period. This would have important implications for empirical glacier melt models calibrated on our melt series (see Section 4.1).

3.3 Atmospheric Circulation

Differenced maps of the 900 hPa geopotential height field for those years with the highest melt deviations are shown in Figure 7, along with the response of the individual SEB components. Four of the high-melt years are characterised by a more southerly flow over western Iceland (1991, 1984, 2003 and 1990), which generally results in an amplification of the temperature-dependent heat fluxes (sensible, latent and longwave energy components). The southerly flow responsible for this enhancement results from different configurations of anomalies in the geopotential height field. In 1984 more southerly flow is a consequence of higher pressure to the south of Iceland, whilst in 1991, 2003 and 1990, low-pressure anomalies to the south/southeast are responsible.

The shortwave heat flux is the main source of melt energy at Vestari Hagafellsjökull, so deviations in this flux have a larger weighting in the overall melt anomaly. This explains why 1987 was characterised by high melt rates, despite the fact that only this flux was markedly enhanced. The pressure field during this year was characterised by a high over the GrIS not unlike that which has been associated with enhanced melting of the ice sheet (Fettweiss et al., 2013). Indeed, 1987 was indeed a warm summer for the south west of the ice sheet (see tables 3 and 4 in Hanna et al. (2014)). Examination of the correlation maps (Figure 8) demonstrates that the net shortwave flux is generally amplified when pressure is higher over the GrIS and lower over North West Europe. These maps also illustrate that, with the exception of the sensible heat flux, the temperature-dependent SEB components are more pronounced when this pressure pattern is reversed.

The detrended melt series are not correlated significantly with the NAOI or GBI at either location (Table 7). For the NAOI this results from the counteracting effects of this index on the temperature-dependent and independent energy fluxes, as the turbulent and longwave SEB components yield correlations with the NAOI which are opposite in sign from that exhibited by net shortwave radiation. The GBI is strongly co-linear with the NAOI (r = -0.86); hence, whilst opposite in sign, the association between the GBI and the SEB components is similar to that exhibited by the NAOI, although generally weaker.

4. Discussion

4.1. Reanalysis climatology and surface energy balance modelling

Comparisons between the reanalysis data and in-situ meteorological measurements indicated appreciable bias, which is consistent with glacier studies elsewhere (e.g. Rye et al., 2010).

303 This is not surprising considering the elevation mismatch between the reanalysis model and 304 our locations (Section 2.3). However, it is unlikely that the bias can be explained only though 305 this elevational discrepancy. For example, the difference in mean air temperatures recorded at 306 VH 500 and the reanalysis data prior to the bias correction is 3.27°C, corresponding to a 307 super-adiabatic mean lapse rate of -2.62°C 100 m^{-1}. Such large biases can instead probably be 308 explained by the glacier's modifying effect on the overlying atmosphere. In being limited to 309 the melting point, glaciers typically have a cooling influence on the air above during melt 310 conditions, simultaneously drying the boundary layer (via condensation) and effecting 311 katabatic winds (Oerlemans, 2010). These processes are essentially microclimatological 312 phenomena unresolved by the reanalysis model. This likely explains the relatively modest 313 association between in-situ and reanalysis wind speeds observed at VH 500, as this location, 314 in being located further along the flowline, is more frequently exposed to katabatic winds 315 (Matthews, 2013), whose variability is partially decoupled from the synoptic wind field 316 (Oerlemans and Grisogono, 2002). The regression model employed in Section 3.1 supports 317 this interpretation. The coefficients indicate that wind speeds at VH 500 increase as ambient 318 air temperature and insolation rise (Table 4). Physically, this is consistent with katabatic 319 forcing because increases in these variables would be expected to amplify the along-glacier 320 pressure gradient, as warmer ambient air temperatures, augmented by solar heating of the 321 glacier environs, create a larger near-surface density gradient (cf. Bjornson et al., 2005).

322 Generally, the empirical corrections applied to the reanalysis data were sufficient to result in 323 good agreement between REF and REANv, which promotes confidence in interpreting 324 changes in potential melt energy given by REANh. This series indicated amplification of 325 nearly all components during the period of simulation with only the longwave flux observed 326 to have remained essentially unchanged, whilst the upward trend in shortwave radiation at 327 VH 500 was of weak significance. The amplification of the turbulent heat fluxes was

particularly compelling, with increases of 28.8 and 61.3% for the sensible and latent heat fluxes, respectively, for VH 500, and increases of 76.9 and 180.9% at VH 1100. This rise can be explained by the trend in air temperatures, which have risen at 0.30 and 0.32°C decade^{-1} at VH 500 and VH 100, respectively, comparable to documented trends in global-scale land surface air temperatures observed during this period (0.25 ± 0.05 °C decade^{-1} to 0.27 ± 0.05 °C decade^{-1}: Jones et al., 2012 and Lawrimore et al., 2011, respectively). The rise in vapour pressure is approximately consistent with what can be expected from theoretical considerations of the effects of warmer air temperatures on the atmosphere's saturation pressure (the Clausius Clapeyron relation: ~7% °C^{-1}), as rates of 6.78 and 5.28% °C^{-1} were observed at VH 500 and VH 1100, respectively.

Although exhibiting an upward trend, the shortwave heat fluxes became less important within the SEB in REAh because their increase did not keep pace with the turbulent heat fluxes. This would have implications for empirical melt models calibrated on our REAh, which are sensitive to the relative melt contributions from different energy fluxes. For example, if the 'degree-day factor' (see e.g. Hock, 2003) is calculated at annual resolution on our series, a significant decrease is observed at VH 1100 (-0.16 mm w.e. d^{-1} °C^{-1} a^{-1}). This trend is consistent with the literature on degree-day factor controls, and their relation to SEB partitioning (Hock, 2003). Whilst a thorough examination of this point is beyond the scope of this paper, it is emphasised that such non-stationarity of SEB components should perhaps be expected at our location, and indeed others, as the climate warms further and the temperature-dependent heat fluxes are enhanced preferentially.

4.2 Atmospheric circulation

Addressing the synoptic dimension to this research, we found that years with the highest melt anomalies were generally characterised by positive deviations of the temperature-dependent heat fluxes resulting from a more southerly flow regime. The recent years characterised by exceptional melting on the GrIS (primarily since 2007) did not register as similarly extreme on Vestari Hagafellsjökull. This can be explained by the fact that the recent high-melt events on the GrIS were a consequence of more persistent anticyclones over the ice sheet (Fettweiss et al., 2013), and such circulation results in northerly flow over Iceland and the advection of a relatively cold air mass (Figure 1). In this regard our study is somewhat consistent with reports of subdued air temperatures and melt rates in Svalbard during the recent period of extreme melting on the GrIS (Moholdt et al., 2010; Kvamstø et al., 2012). Our results therefore add to the consensus that, when atmospheric ridging over Greenland is pronounced, the vigorous melting observed over the GrIS does not extend east of the ice sheet in this region of the North Atlantic.

Greater insight into synoptic controls on the SEB was granted through correlation analysis and the clearest associations with the 900 hPa flow field were observed for the radiative and latent heat fluxes. The shortwave energy flux indicated a tendency to be enhanced when the pressure field drives north-easterly flow, in a configuration opposite to that favoured by the longwave and latent heat fluxes. These correlation fields show a high degree of similarity to the dipole structure of the summertime NAO, which has positive and negative centres over northwest Europe and Greenland, respectively (Folland et al., 2009), hinting at the importance of the NAO in modulating surface energetics which was confirmed by inspection of the NAOI time series.

When the summertime NAO is in a positive phase, circulation is more anticyclonic over the northwest Europe and more cyclonic over Iceland/southeast Greenland. This results in southerly flow over a warm ocean surface, advecting a humid air mass over Vestari Hagafellsjökull and explaining the positive correlation between the NAOI and the latent and longwave heat fluxes (which depend on the atmospheric vapour pressure). The storm tracks also pass close to Iceland during this phase of the NAO (Folland et al., 2009), which would enhance cloud cover over our study site and explains further the correspondence with the longwave heat flux (which also depends on cloud cover: Sedlar and Hock (2009)). During the negative phase of the summertime NAO, these conditions are reversed: circulation is more anticyclonic over Iceland and the storm tracks pass to the south, explaining the enhanced insolation for Vestari Hagafellsjökull inferred from our study.

It is a consequence of the opposing sign of the correlations with the NAOI for the temperature dependent and independent SEB components, that melt itself is not correlated significantly with this index. This cancelling effect is also evident in Figure 8, where only the sensible heat flux correlation is ‘carried through’ to the melt correlation map, as it hasn’t been cancelled by a spatially-coincident correlation of opposite sign. We also observed that the NAOI is almost universally better correlated with the SEB components than the GBI. This may be because the NAOI expresses the strength of the dipole pattern, which probably carries more information about resulting circulation over this region of the North Atlantic (and air mass advection over Vestari Hagafellsjökull) than the GBI, which emphasises the northern centre of the dipole (Fang, 2004).

5. Conclusions

The main aims of this study were to assess the feasibility of simulating potential glacier surface melt energy with bias corrected reanalysis data, and to evaluate the role of synoptic circulation in modulating the surface energetics. Our conclusions from this work can be summarised:

1) Using only simple empirical corrections, the ERA-Interim data captured an encouraging amount of variance in the observed SEB. Accordingly, we conclude that

this technique holds promise for hindcasting series of glacier-surface meteorology and potential melt energy.

2) Potential melt energy has increased significantly over the period 1979-2012, primarily as a result of a rise in air temperature. Because the different energy fluxes have not increased at a uniform rate the relative partitioning of melt energy has also changed, with the turbulent heat fluxes becoming significantly more important.
3) Generally, southerly air flow was observed to drive the highest melt rates on Vestari Hagafellsjökull through amplification of the temperature-dependent heat fluxes. As the recent atmospheric ridging over Greenland (which has been associated with the remarkable melting of the ice sheet) induces a northerly flow over Iceland, similarly anomalous melt rates have not been experienced for our Icelandic glacier during these recent years.
4) The NAO is an important control on the SEB, particularly the radiative heat fluxes. Positive correlations were observed for the NAOI with the temperature-dependent heat fluxes, whilst the net shortwave heat flux exhibited a negative correlation. Because these correlations are opposite in sign they cancel each other out, resulting in no significant association between melt itself and the NAOI. The role of the NAO in modulating surface energetics would therefore not have emerged in our study if the integrated melt response to synoptic forcing had been assessed in isolation.

We conclude that the approach adopted here provides an important means of understanding the coupling between local-scale glacier melt processes and synoptic-scale climate variability, which is required in understanding the response of glaciers to climate change.

References

Arendt A and Sharp MJ. 1999. Energy balance measurements on a Canadian high arctic glacier and their implications for mass balance modeling. *IAHS Publication* **256**: 165-172

Beyene T, Lettenmaier D and Kabat P. 2010. Hydrologic impacts of climate change on the Nile River Basin: implications of the 2007 IPCC scenarios. *Climatic Change* **100**: 433–461. DOI: 10.1007/s10584-009-9693-0

Björnsson H, Guðmundsson S, and Pálsson F. 2005. Glacier winds on Vatnajökull ice cap, Iceland, and their relation to temperatures of its lowland environs. *Annals of Glaciology* **42**: 291-296

Boé J, Terray L, Habets F and Martin E. 2007. Statistical and dynamical downscaling of the Seine basin climate for hydro-meteorological studies. *International Journal of Climatology* **27**: 1643–1655. DOI:10.1002/joc.1602

Box JE. 2002. Survey of Greenland instrumental temperature records: 1873–2001. *International Journal of Climatology* **22**: 1829-1847. DOI: 10.1002/joc.852

Bradley RS, Vuille M, Diaz HF and Vergara W. 2006. Threats to water supplies in the tropical Andes. *Science* **312**: 1755-1756. DOI: 10.1126/science.1128087

Braithwaite RJ. 1995. Positive degree-day factors for ablation on the Greenland ice sheet studied by energy balance modeling. *Journal of Glaciology* **41**: 153-160

Brazel AJ, Chambers FB and Kalkstein LS. 1992. Summer energy balance on West Gulkana Glacier, Alaska, and linkages to a temporal synoptic index. *Zeitschrift für Geomorphologie* **86**: 15-34 de Wildt MDR, Oerlemans J and Björnsson H. 2004. A calibrated mass balance model for Vatnajökull. *Jökull* **52**: 1-20

Dee DP, Uppala SM, Simmons AJ, Berrisford P, Poli P, Kobayashi S, Andrae U, Balmaseda MA, Balsamo G, Bauer P, Bechtold P, Beljaars ACM, Van de Berg L, Bidlot J, Bormann N, Delsol C, Dragani R, Fuentes M, Geer AJ, Haimberger L, Healy SB, Hersbach H, Hólm EV, Isaksen L, Kållberg P, Köhler M, Matricardi M, Mcnally AP, Monge-sanz BM, Morcrette J, Park B, Peubey C, de Rosnay P, Tavolato C, Thépaut J and Vitart F. 2011. The ERA-Interim reanalysis: configuration and performance of the data assimilation system. *Quarterly Journal of the Royal Meteorological Society* **137**: 553-597. DOI: 10.1002/qj.828

Dobler C, Hagemann S, Wilby RL and Stötter J. 2012. Quantifying different sources of uncertainty in hydrological projections in an Alpine watershed. *Hydrology & Earth System Sciences* **16**: 4343–4360. DOI: 10.5194/hess-16-4343-2012

Einarsson MÁ. 1984. *Climate of Iceland*. In: Van Loon H. ed. *Climates of the Oceans.* First edn. Amsterdam: 673-697

Fang ZF. 2004. Statistical relationship between the northern hemisphere sea ice and atmospheric circulation during wintertime. In *Observation, Theory and Modeling of Atmospheric Variability. World Scientific Series on Meteorology of East Asia*, Zhu X (ed). World Scientific Publishing Company: Singapore; 131–141

Fettweis X, Mabille G, Erpicum M, Nicolay S and Broeke M. 2011. The 1958-2009 Greenland ice sheet surface melt and the mid-tropospheric atmospheric circulation. *Climate Dynamics* **36**: 139-159. DOI: 10.1007/s00382-010-0772-8

Fettweis X, Hanna E, Lang C, Belleflamme A, Erpicum M and Gallée H. 2013. Brief communication: Important role of the mid-tropospheric atmospheric circulation in the recent surface melt increase over the Greenland ice sheet. *The Cryosphere* **7**: 241-248. DOI: 10.5194/tc-7-241-2013

Folland CK, Knight J, Linderholm HW, Fereday D, Ineson S and Hurrell JW. 2009. The summer North Atlantic Oscillation: past, present, and future. *Journal of Climate* **22**: 1082-1103. DOI: 10.1175/2008JCLI2459.1

Giesen RH, Andreassen LM, Broeke MR and Oerlemans J. 2009. Comparison of the meteorology and surface energy balance at Storbreen and Midtdalsbreen, two glaciers in southern Norway. *The Cryosphere* **3**: 57-74. DOI: 10.5194/tc-3-57-2009

Gudmundsson L, Bremnes JB, Haugen JE and Engen-Skaugen T. 2012. Technical Note: Downscaling RCM precipitation to the station scale using statistical transformations--a comparison of methods. *Hydrology & Earth System Sciences* **16**: 3383-3390. DOI: 10.5194/hess-16-3383-2012

Guðmundsson S, Björnsson H, Pálsson F and Haraldsson HH. 2009. Comparison of energy balance and degree-day models of summer ablation on the Langjökull ice cap, SW-Iceland. *Jökull* **59**: 1-17

Hanna E, Fettweis X, Mernild SH, Cappelen J, Ribergaard MH, Shuman CA and Mote TL. 2014. Atmospheric and oceanic climate forcing of the exceptional Greenland ice sheet surface melt in summer 2012. *International Journal of Climatology* **34**: 1022-1037. DOI: 10.1002/joc.3743

Hanna E, Jónsson T and Box JE. 2004. An analysis of Icelandic climate since the nineteenth century. *International Journal of Climatology* **24**: 1193-1210. DOI: 10.1002/joc.1051

Hanna E, Jones JM, Cappelen J, Mernild SH, Wood L, Steffen K, Huybrechts, P. 2013. The influence of North Atlantic atmospheric and oceanic forcing effects on 1900-2010 Greenland summer climate and ice melt/runoff. *International Journal of Climatology* **33**: 862-880. DOI: 10.1002/joc.3475

Hannah DM, Gurnell AM and Mcgregor GR. 1999. Identifying links between large-scale atmospheric circulation and local glacier ablation climates in the French Pyrenees. *IAHS Publication* **256**: 155-164

Hashino T, Bradley AA and Schwartz SS. 2007. Evaluation of bias-correction methods for ensemble streamflow volume forecasts. *Hydrology & Earth System Sciences* **11**: 939-950. DOI: 10.5194/hess-11-939-2007

Hay JE and Fitzharris BB. 1988. A comparison of the energy balance and bulk - aerodynamic approaches for estimating glacier melt. *Journal of Glaciology* **34**: 144-153

Hock R. 2003. Temperature index melt modelling in mountain areas. *Journal of Hydrology* **282**: 104-115. DOI: 10.1016/s0022-1694(03)00257-9

Hock R, Radic V and de Woul M. 2007. Climate sensitivity of Storglaciären, Sweden: an intercomparison of mass-balance models using ERA-40 re-analysis and regional climate model data. *Annals of glaciology* **46**: 342-348. DOI: 10.3189/172756407782871503

Hock R and Holmgren B. 2005. A distributed surface energy balance model for complex topography and its application to Storglaciären, Sweden. *Journal of Glaciology* **51**: 25-36. DOI: 10.3189/172756505781829566

Jacob T, Wahr J, Pfeffer WT and Swenson S. 2012. Recent contributions of glaciers and ice caps to sea level rise. *Nature* **482**: 514-518. DOI: 10.1038/nature10847

Jones PD. Lister DH. Osborn TJ. Harpham C. Salmon M. and Morice CP. 2012. Hemispheric and large-scale land-surface air temperature variations: An extensive revision and an update to 2010. *Journal of Geophysical Research: Atmospheres* **117**.

Jansson P, Hock R and Schneider T. 2003. The concept of glacier storage: a review. *Journal of Hydrology* **282**: 116-129. DOI: 10.1016/S0022-1694(03)00258-0

Jarosch AH, Anslow FS and Clarke GK. 2012. High-resolution precipitation and temperature downscaling for glacier models. *Climate Dynamics*, **38**: 391-409. DOI: 10.1007/s00382-010-0949-1

Klok EJ and Oerlemans J. 2002. Model study of the spatial distribution of the energy and mass balance of Morteratschgletscher, Switzerland. *Journal of Glaciology* **48**: 505-518. DOI: 10.3189/172756502781831133

Konya K and Matsumoto T. 2010. Influence of weather conditions and spatial variability on glacier surface melt in Chilean Patagonia. *Theoretical Applied Climatology* **102**: 139-149. DOI: 10.1007/s00704-009-0248-0

Kvamstø NG. Steinskog DJ. Stephenson DB. and Tjøstheim DB. 2012. Estimation of trends in extreme melt-season duration at Svalbard. *International Journal of Climatology*, **32**: 2227-2239. DOI: 10.1002/joc.3395

Lawrimore JH. Menne MJ. Gleason BE. Williams CN. Wuertz DB. Vose RS. and Rennie J. 2011. An overview of the Global Historical Climatology Network monthly mean temperature data set, version 3. *Journal of Geophysical Research* **116**. DOI: 10.1029/2011JD016187

Matthews TKR. 2013. *Glacier-climate interactions: a synoptic approach.* PhD thesis, Loughborough University. Available at: https://dspace.lboro.ac.uk/2134/12558.

Matthews T, Hodgkins R, Wilby RL, Guðmundsson S, PálssonF, Björnsson H, and Carr S. 2014. Conditioning temperature-index model parameters on synoptic weather types for glacier melt simulations. *Hydrological Processes*. DOI: 10.1002/hyp.10217

Meier MF, Dyurgerov MB, Rick UK, O'Neel S, Pfeffer WT, Anderson RS, Anderson SP and Glazovsky AF. 2007. Glaciers dominate eustatic sea-level rise in the 21st century. *Science* **317**: 1064. DOI: 10.1126/science.1143906

Moholdt G. Nuth C. Hagen JO. and Köhler, J. 2010. Recent elevation changes of Svalbard glaciers derived from ICESat laser altimetry. Remote Sensing of Environment. **114**: 2756–2767. DOI:10.1016/j.rse.2010.06.008

Nicholson L, Prinz R, Mölg T, and Kaser G. 2012. Micrometeorological conditions and surface mass and energy fluxes on Lewis glacier, Mt Kenya, in relation to other tropical glaciers. *The Cryosphere* **7**: 5181-5224. DOI: 10.5194/tc-7-1205-2013

Oerlemans J. 2010. *The microclimate of valley glaciers*. First edn. Utrecht: Igitur, Utrecht Publishing and Archiving Services, Universiteitsbibliotheek Utrecht

Oerlemans J. 2000. Analysis of a 3 year meteorological record from the ablation zone of Morteratschgletscher, Switzerland: energy and mass balance. *Journal of Glaciology* **46**: 571-579. DOI: 10.3189/172756500781832657

Oerlemans J and Grisogono B. 2002. Glacier winds and parameterisation of the related surface heat fluxes. *Tellus A* **54**: 440-452. DOI: 10.1034/j.1600-0870.2002.201398.x

Radić V and Hock R. 2006. Modelling future glacier mass balance and volume changes using ERA-40 reanalysis and climate models: A sensitivity study at Storglaciären, Sweden, *Journal of Geophysical Research: Earth Surface* **111**. DOI: 10.1029/2005JF000440

Rye CJ, Arnold NS, Willis IC. and Kohler J. 2010. Modeling the surface mass balance of a high Arctic glacier using the ERA-40 reanalysis. *Journal of Geophysical Research*: *Earth Surface* **115**. DOI: 10.1029/2009JF001364

Sedlar J and Hock R. 2009. Testing longwave radiation parameterizations under clear and overcast skies at Storglaciaren, Sweden. *The Cryosphere* **3**: 75-84. DOI: 10.5194/tc-3-75-2009

Sicart JE, Hock R, Ribstein P, Litt, M and Ramirez E. 2011. Analysis of seasonal variations in mass balance and meltwater discharge of the tropical Zongo Glacier by application of a distributed energy balance model. *Journal of Geophysical Research: Atmospheres* **116**. DOI: 10.1029/2010JD015105

Six D, Wagnon P, Sicart JE and Vincent C. 2009. Meteorological controls on snow and ice ablation for two contrasting months on Glacier de Saint-Sorlin, France. *Annals of glaciology* **50**: 66-72. DOI: 10.3189/172756409787769537

Themeßl MJ, Gobiet A and Heinrich G. 2012. Empirical-statistical downscaling and error correction of regional climate models and its impact on the climate change signal. *Climatic Change* **112**: 449–468. DOI:10.1007/s10584-011-0224-4

Wang CC and Rogers JC. 2001. A Composite Study of Explosive Cyclogenesis in Different Sectors of the North Atlantic. Part I: Cyclone Structure and Evolution. *Monthly Weather Review* **129**: 1481-1499. DOI: 10.1175/1520-0493(2001)129<1481:ACSOEC>2.0.CO;2

Zhang J, Bhatt US, Tangborn WV and Lingle CS. 2007. Climate downscaling for estimating glacier mass balances in northwestern North America: Validation with a USGS benchmark glacier. *Geophysical Research Letters* ***34***. DOI: 10.1029/2007GL031139

Figure captions:

Table 7. Correlations, and their significance, between REANh and the NAOI and GBI. Note that p is the probability of obtaining a correlation coefficient as large (in an absolute sense) as that given if the null hypothesis (that $r = 0$) is true

Figure 1. Location of study sites. Right-hand-side shows the climatological setting of Iceland, in terms of near-surface air temperatures (top) and sea surface temperatures (bottom). The air temperatures were obtained from the 1981-2010 NCEP1 climatology (Kalanay et al., 1996) and the sea surface temperatures were calculated by averaging the long-term monthly mean values over the period 1971-2000 from the NOAA_OI_SST_V2 dataset, provided by the NOAA/OAR/ESRL PSD (http://www.esrl.noaa.gov/psd/)**.** Left-hand-side: the Langjökull ice cap and its situation within Iceland (inset). The locations of the two AWSs (VH 500 and VH 1100) are also indicated

Figure 2. Empirical cumulative distributions for the observed and reanalysis variables. Note that the reanalysis variables have been bilinearly interpolated to the location of the AWSs

Figure 3. Comparisons between the REF and REANv series when compared at daily (top) and annual (bottom) resolution. Note that correlation coefficients quantifying the linear relationship between these series are provided in Table 4. Energy fluxes in the legend are abbreviated as follows: SHF: sensible heat flux, LHF: latent heat flux, SW: net shortwave radiation and LW: net longwave radiation

Figure 4. The hindcast SEB series. Hindcast fluxes and melt are shown annually (JJA); the totals are derived by summing all daily JJA contributions to melting for each year. Error bars for each series indicate ±1 standard deviation of the residuals for annual totals when compared to REF, deduced from inspecting the series illustrated in Figure 3. The dotted lines were fit with linear regression: see Table 6 for their slopes and significance. Energy fluxes are abbreviated as outlined in Figure 3 caption

Figure 5. Annual (JJA) contributions of each of the energy fluxes to total melt at both elevations during the hindcasting period (1979-2012), illustrating the relative contribution to melting from each of the energy fluxes

Figure 6. The fraction (expressed as a percentage) of total annual melt energy (JJA) provided by the turbulent heat fluxes (sensible + latent), relative to that contributed by the radiative heat fluxes (shortwave + longwave). The dotted lines indicate the least-squares linear fit. The trends are both significant (at $p = 0.05$) according to a two-tailed *t*-test. Uncertainty bars (±δ) are calculated: $\delta = \sqrt{\left[\frac{\delta SHF^2+\delta LHF^2}{(SHF+LHF)^2}\right]+\left[\frac{\delta SW^2+\delta LW^2}{(SW+LW)^2}\right]}\ K$, where K is the fraction plotted and the errors terms for the individual energy components (δx), are denoted as given in Figure 3 caption, and whose values were estimated as outlined in the caption of Figure 4

Figure 7. Anomaly maps for the five years with the highest melt rate (see Section 2.5). Left-hand-side: the 900 hPa height (colormap), and wind vector anomalies (arrows). Because the gridded data are linearly detrended, the anomaly fields plotted for each JJA period were calculated simply by averaging the grid-point values for the year in question (as the detrended gridpoint series have means of zero). The 'u' and 'v' wind vectors required for this plot were obtained from the ERA-Interim archive as monthly means of daily means. Right-hand-side: contributions to melting from the detrended components of the REANh series for JJA in the years indicated

Figure 8. Correlations (ρ), at annual (JJA) resolution, between components of REANh and the 900 hPa height field. The white line bounds correlations that are significantly different from zero at p <0.05. Note that all series are detrended with respect to time. Energy flux abbreviations are outlined in Figure 3 caption

Table 1. Meteorological variables required for the SEB model (described in the text and in Table 2), and the meteorological variables used from the ERA-Interim archive to satisfy these requirements. The column labelled 'transformations' details the relevant treatment applied to the reanalysis variables needed to maintain compatibility with the required input variable

Required input variable	**Reanalysis variable used**	**Transformation**
Two-metre air temperature	Two-metre air temperature	*NA*
Two-metre vapour pressure (e)	Two-metre dewpoint temperature (T_d)	$e = e_0\, exp[-(\frac{1}{T_d} - \frac{1}{T_0})\, L\, RV^{-1}]$ with e_0 = 610.8 Pa; $T_0 = 273.15K$; L = the latent heat of vaporization (2.5 × 10^6 J kg^{-1}); RV = the gas constant for water vapour (461 J kg^{-1}). Note that T_d is in Kelvin.
Two-metre wind speed (W_s)	10-metre U-component (U) of wind speed; 10-metre V-component (V) of wind speed	$W_s = \sqrt{U^2 + V^2}$
Incident shortwave radiation	Surface solar radiation downwards	*NA*
Incident longwave radiation	Surface thermal radiation downwards	*NA*

Table 2. Details of energy fluxes' treatment within the SEB model. See text in Section 2.4 for further explanation

Model for calculating the SEB (Q):

$$Q = Q_H + Q_L + Q_{SW} + Q_{LW} + Q_R + Q_G$$

Quantity	Procedure for calculation	Associated parameters/ parameterisations	Treatment/value of parameters
Turbulent heat (sensible: Q_H and latent: Q_L heat)	Bulk aerodynamic method	Roughness length of momentum	Ice: 10 mm Firn: 2 mm Snow: 0.1 mm
		Roughness lengths of water vapour and temperature	Modelled according to Andreas (1987).
		Stability corrections for turbulent heat flux calculations	Non-linear expressions of Beljaars and Holtslag (1991) used for stable conditions (glacier surface temperature below air temperature); equations of Paulson (1970) and Dyer (1974) applied for unstable case.
		Glacier surface temperature	Assumed to be at the melting point (0°C).
Net shortwave (Q_{SW})	Incident flux minus reflected flux	Reflected shortwave radiation	Taken from measurements during period when the reanalysis-driven SEB is validated; calculated by multiplying the incident flux by the mean observed albedo during the measurement period for the hindcasting experiment (1979-2012). See text for more details.
Net longwave (Q_{LW})	Incident flux minus the flux emitted by the glacier surface	Emitted longwave radiation	Measured values used during validation period; emission assumed equal to a blackbody at the melting point during the hindcasting experiment.
Rain (Q_R) and Ground (Q_G)	*Neglected*	*Neglected*	*Neglected*

Table 3. Correlation coefficients between the daily mean values of the meteorological variables observed at the AWSs, and the bias-corrected (quantile-mapped) ERA-Interim reanalysis variables. Note that all correlations are highly significant (p <0.01)

	VH 500	VH 1100
Air temperature	0.73	0.88
Wind speed	0.50	0.67
Vapour pressure	0.77	0.85
Incident shortwave radiation	0.78	0.79
Incident longwave radiation	0.76	0.67

Table 4. Details of the regression model used to correct the bias corrected reanalysis wind speed at VH 500. Note that *t* is the student's *t*-statistic, and *p* indicates the probability of obtaining an absolute value of *t* larger than given in the preceding column if the null hypothesis (that $\beta_i = 0$) is true

Regression model summary: Glacier wind speed can be written: $Wspd_{ERA\_bc}$ - y; where $Wspd_{ERA\_bc}$ is the bias-corrected ERA-Interim wind speed and 'y' is $Wspd_{ERA\_bc}$ minus the observed glacier wind speed. 'y' can be written: $y = \beta_0 x_0 + \beta_1 x_1 + \beta_2 x_2 + \epsilon$, where x_i are variables, β_i are regression coefficients and ϵ is a random error term. Below, values of the regression coefficients used to estimate 'y' are provided.

Variable: x_i	**Coefficient: β_i (units)**	***t***	***p***
Constant ($x_0 = 1$)	3.9713 (m s^{-1})	14.56	0.00
Raw ERA-Interim 2-metre air temperature (x_1)	-0.3490 (m s^{-1} °C^{-1})	-11.41	0.00
Bias-corrected ERA-Interim incident shortwave radiation (x_2)	-0.0060 (m s^{-1} W^{-1} m^2)	-9.07	0.00
			N = 642; Adj. R^2 = 0.28

Table 5. Relative contribution (%) to melting of the energy fluxes calculated with SEB when forced with in-situ AWS observations (REF) and with the bias-corrected ERA-Interim reanalysis data (REANv). Correlation coefficients between the REANv and REF series are also given, which are nearly all significant at p <0.01; those correlations that are not significant at the 99% confidence interval for a two-tailed t-test are marked with asterisks: *is significant at the 95% confidence interval (p = 0.02); ** is not significant at the 90% confidence interval (p = 0.11). Note that REANv is calculated using a regression-based correction to the wind speed at VH 500 (see text in Section 3.1 and Table 4)

	VH 500				**VH 1100**			
	REF (%)	REANv (%)	r (daily)	r (annual)	REF (%)	REANv (%)	r (daily)	r (annual)
Sensible Heat	26.96	27.45	0.78	0.82*	19.81	20.05	0.74	0.84
Latent heat	9.83	10.35	0.81	0.65**	6.03	6.18	0.74	0.84
Shortwave radiation	63.92	62.89	0.79	0.93	92.03	89.16	0.84	0.98
Longwave radiation	-0.71	-0.69	0.75	0.95	-17.88	-15.39	0.55	0.90
Melt	-	-	0.79	0.98	-	-	0.87	0.96

Table 6. REANh trends and their significance (*p*) during the hindcasting period (1979-2012). See the text in Section 2.4 for further details

	VH 500		1100 m	
	slope (mm w.e. a^{-2})	*p*	slope (mm w.e. a^{-2})	*p*
Sensible heat flux	11.68	0.00	6.51	0.00
Latent heat flux	7.46	0.01	2.81	0.05
Net shortwave radiation	10.94	0.16	7.79	0.05
Net longwave radiation	1.40	0.63	-0.95	0.72
Melt	31.47	0.00	16.15	0.01

Table 7. Correlations, and their significance, between REANh and the NAOI and GBI. Note that *p* is the probability of obtaining a correlation coefficient as large (in an absolute sense) as that given if the null hypothesis (that $r = 0$) is true

	SEB Component	**NAOI**		**GBI**	
		r	*p*	*r*	*p*
VH 500	Sensible heat flux	0.12	0.50	0.05	0.78
	Latent heat flux	0.30	0.08	-0.08	0.66
	Net shortwave radiation	-0.66	0.00	0.54	0.00
	Net longwave radiation	0.46	0.01	-0.23	0.20
	Melt	-0.20	0.26	0.33	0.06
VH 1100	Sensible heat flux	0.05	0.78	0.17	0.33
	Latent heat flux	0.40	0.02	-0.15	0.38
	Net shortwave radiation	-0.51	0.00	0.53	0.00
	Net longwave radiation	0.51	0.00	-0.34	0.05
	Melt	0.04	0.80	0.18	0.31

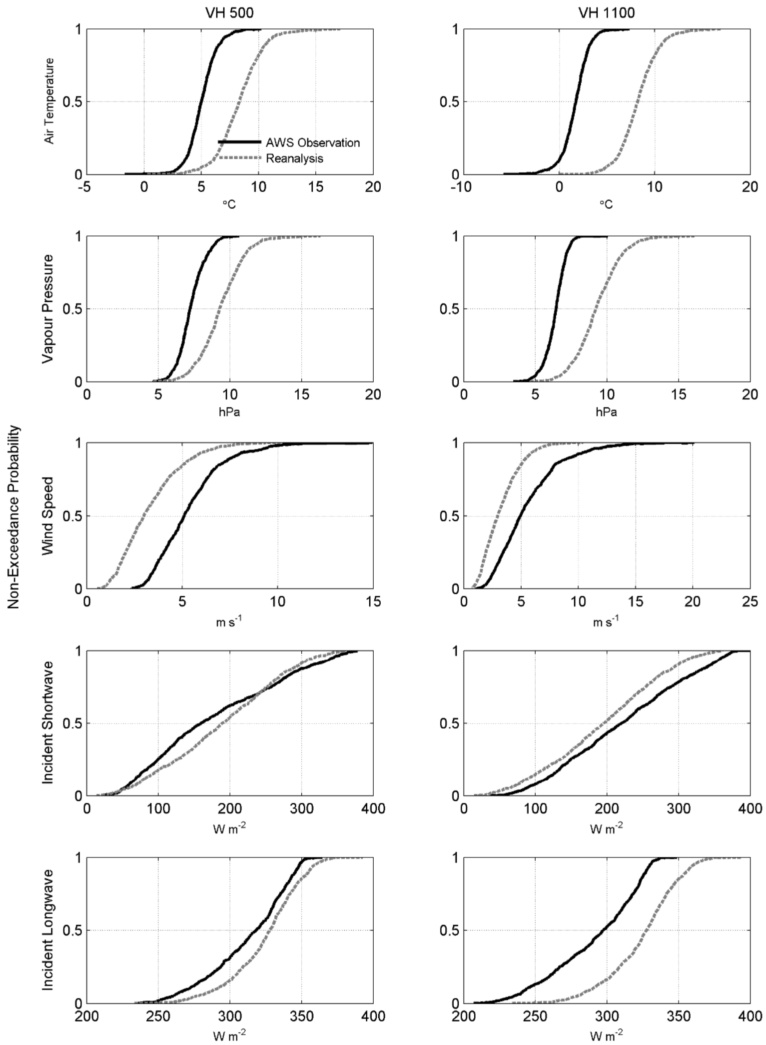

205x287mm (300 x 300 DPI)

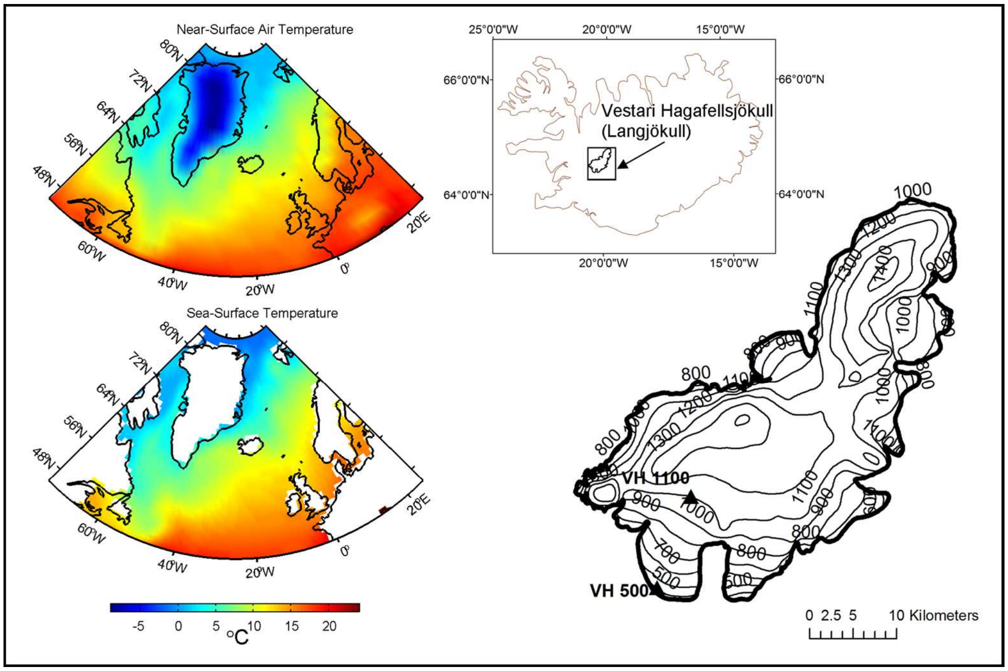

166x110mm (300 x 300 DPI)

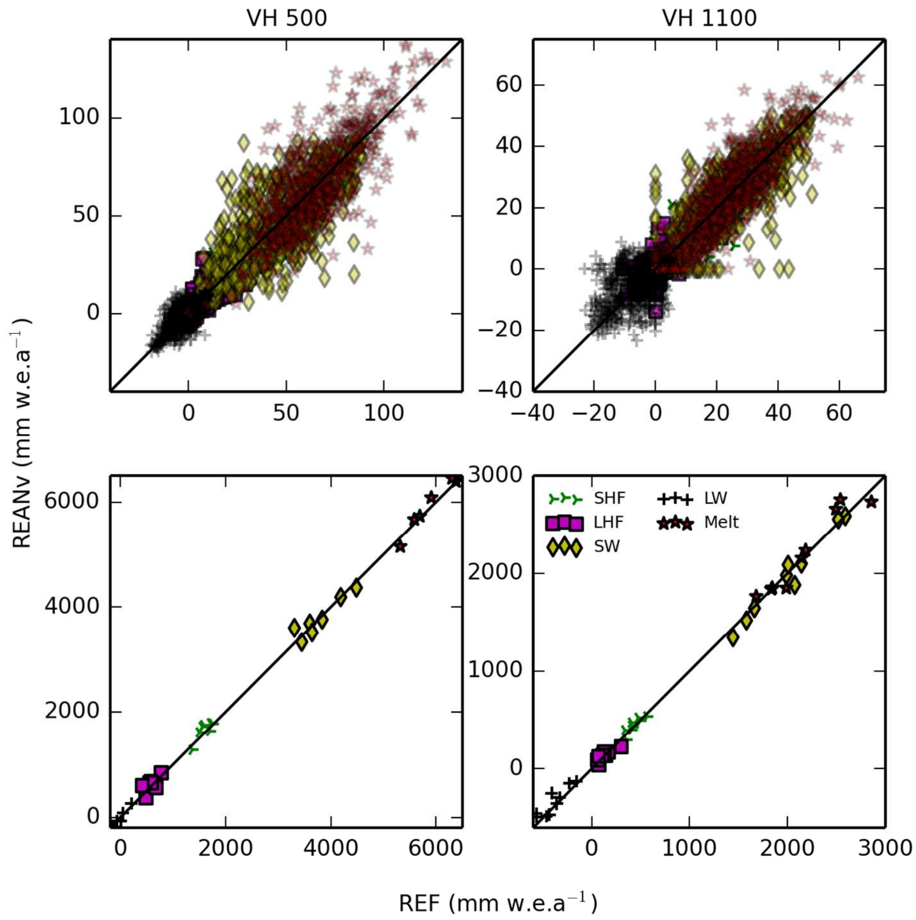

127x127mm (300 x 300 DPI)

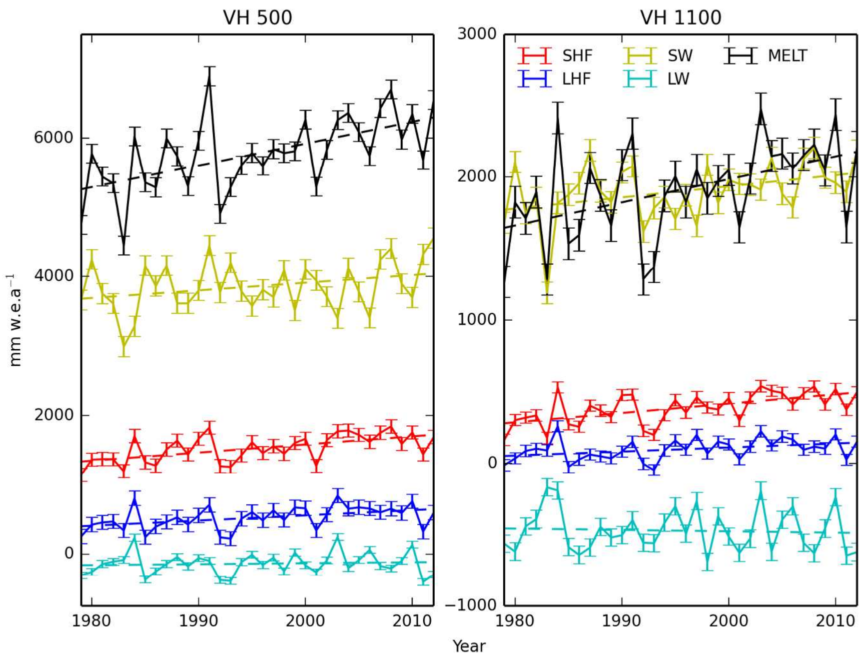

177x127mm (300 x 300 DPI)

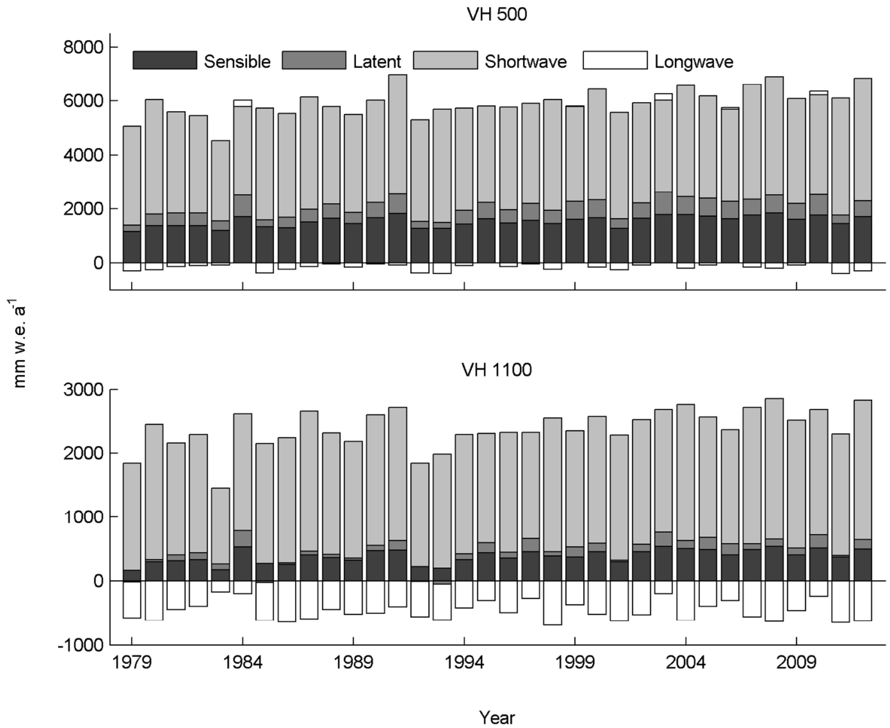

160x120mm (300 x 300 DPI)

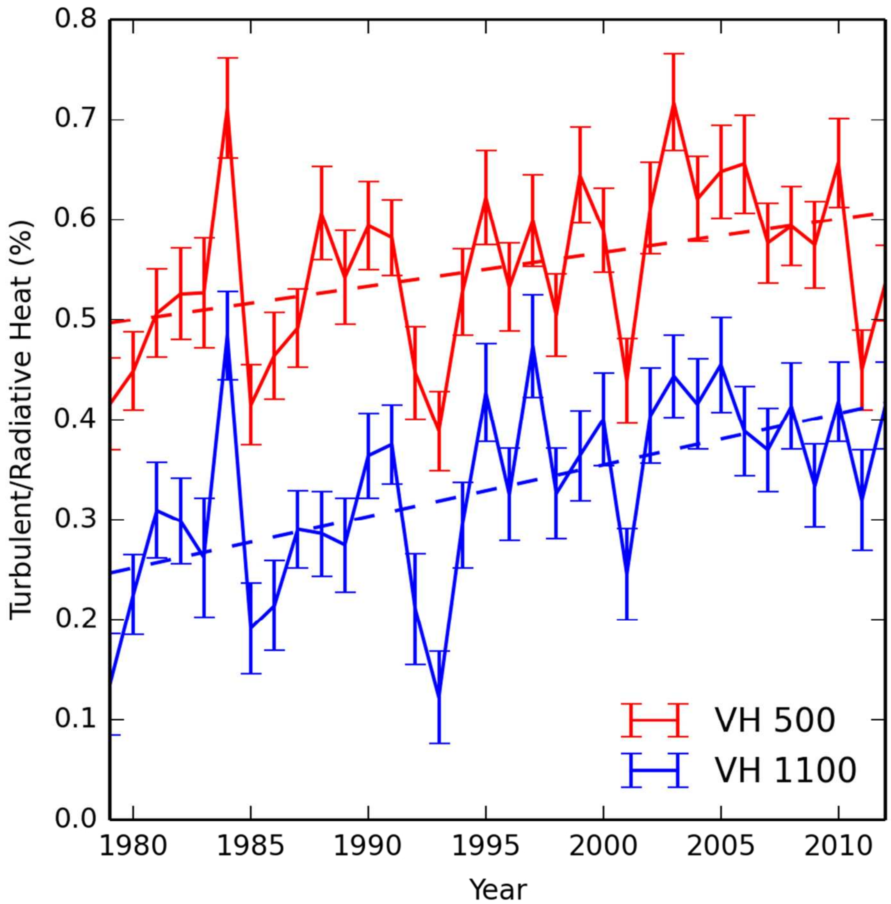

101x101mm (300 x 300 DPI)

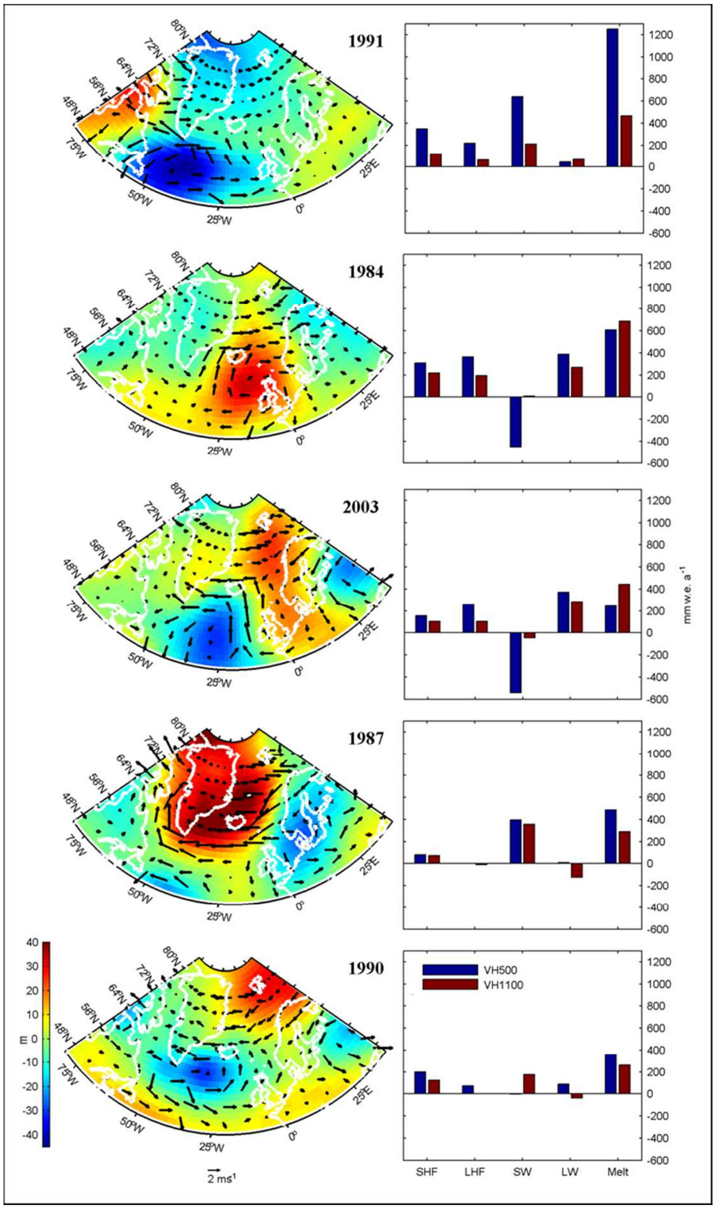

138x234mm (150 x 150 DPI)

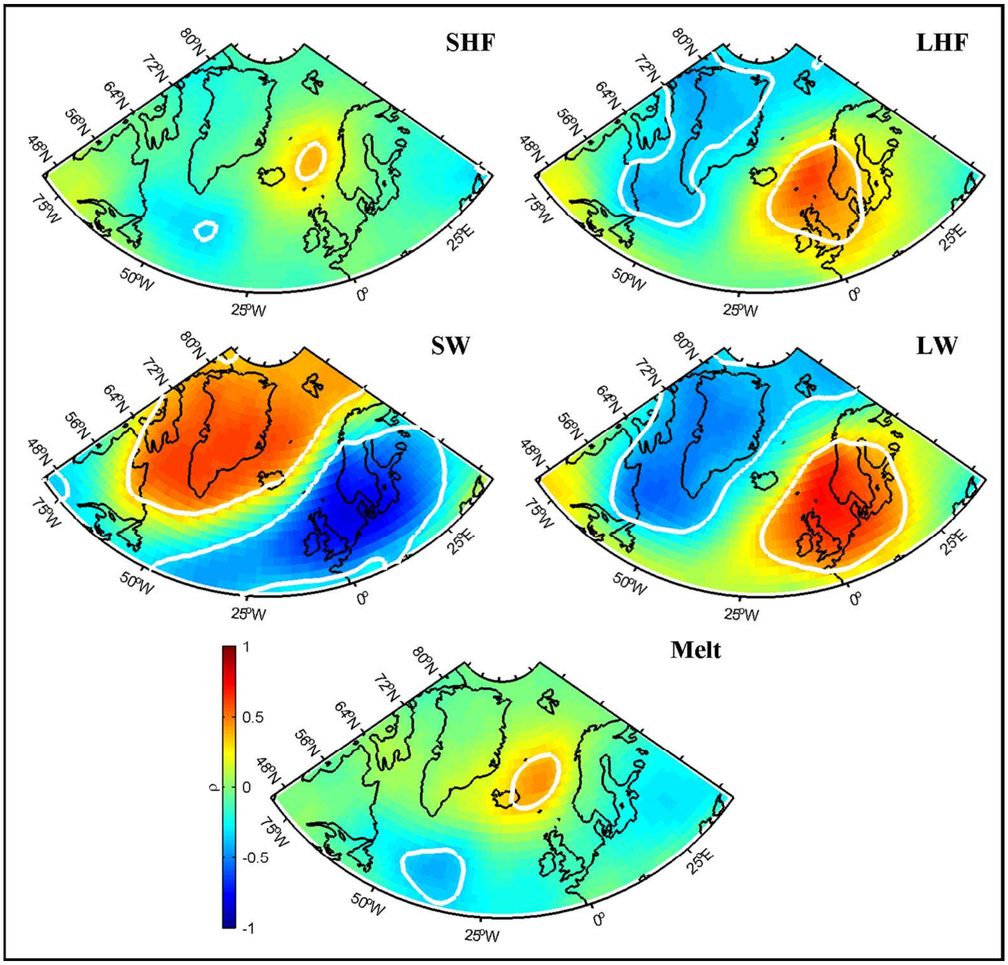

138x132mm (300 x 300 DPI)